Journal of Sound and Vibration 331 (2012) 704–720

Contents lists available at SciVerse ScienceDirect

Journal of Sound and Vibration

journal homepage: www.elsevier.com/locate/jsvi

Vibrations of post-buckled rods: The singular inextensible limit

Sébastien Neukirch [a,b,*], Joël Frelat [a,b], Alain Goriely [c], Corrado Maurini [a,b]

[a] CNRS, UMR 7190, Institut Jean Le Rond d'Alembert, F-75005 Paris, France
[b] UPMC Univ Paris 06, UMR 7190, Institut Jean Le Rond d'Alembert, F-75005 Paris, France
[c] Oxford Centre for Collaborative Applied Mathematics (OCCAM), Oxford University, UK

ARTICLE INFO

Article history:
Received 11 May 2011
Received in revised form
27 September 2011
Accepted 27 September 2011
Handling Editor: L.N. Virgin
Available online 14 October 2011

ABSTRACT

The small-amplitude in-plane vibrations of an elastic rod clamped at both extremities are studied. The rod is modeled as an extensible, shearable, planar Kirchhoff elastic rod under large displacements and rotations, and the vibration frequencies are computed both analytically and numerically as a function of the loading. Of particular interest is the variation of mode frequencies as the load is increased through the buckling threshold. While for some modes there are no qualitative changes in the mode frequencies, other frequencies experience rapid variations after the buckling threshold, the thinner the rod, the more abrupt the variations. Eventually, a mismatch for half of the frequencies at buckling arises between the zero thickness limit of the extensible model and the inextensible model.

1. Introduction

The first step in the study of vibrating elastic structures [1] focuses on the dynamical response of the system around its unstressed configuration. In vibration analysis, the dynamics of infinitely small-amplitude disturbances around the fundamental equilibrium state are generally first considered, leading to a linear problem. However, nonlinear effects are known to play a key role in many elastic systems, and in the context of vibrations, nonlinearities can be included by studying large-amplitude oscillations around the fundamental state [2]. The second step in the analysis of vibrations is to study the effect of external loads. They have a direct influence on the dynamical response of the system, as easily demonstrated by tuning the natural frequencies of a string by putting it under tension. Similarly, in compression, the natural frequencies of a rod decrease. Again nonlinear effects become important when external loads not only change the vibration response of the rod but also alter its overall stability through buckling. Several studies have investigated dynamical responses of post-buckled elastic rods around their post-buckled state, see e.g. Chapter 12 of [1] and [3–5]. The present work also focuses on the problem of small-amplitude vibrations around a pre-strained deformed nonlinear elastic rod, and shows that vibration frequencies behave singularly at buckling. This problem is relevant for a number of applications including the manufacturing of piano (or violin) soundboards where the wooden board is bent before being clamped in the rigid metal frame [6–8]. Other systems where pre-stress and/or pre-strain play an important role for the vibration response are gongs, cymbals, and steel drums where plastic deformations of the metal plates are used to introduce separation of response modes [9].

Here, we consider the problem of in-plane vibrations of a pre- and post-buckled Kirchhoff extensible shearable elastic rod. First, we study the equilibrium configurations of a clamped–clamped rod as the ends are gradually moved together.

* Corresponding author at: UPMC Univ Paris 06, UMR 7190, Institut Jean Le Rond d'Alembert, F-75005 Paris, France.
E-mail address: sebastien.neukirch@upmc.fr (S. Neukirch).

0022-460X/$ - see front matter © 2011 Elsevier Ltd. All rights reserved.
doi:10.1016/j.jsv.2011.09.021

The rod has a straight natural shape and for small axial displacements the rod remains straight until a critical displacement is reached where the rod buckles in the plane. For each value of the axial displacement we study the small-amplitude vibrations around the equilibrium state and we follow how frequencies of the natural modes change as the load is increased. For both equilibrium and vibrations we enforce displacement control boundary conditions, that is, the axial displacement rather than the axial load is imposed.

The paper is organized as follows: In Section 2 we present Kirchhoff model for elastic rods, in Section 3 we derive the equations for the small-amplitude vibrations of a rod around its post-buckled equilibrium. We compute equilibriums in Section 4, vibrations in the extensible case in Section 5 and in the extensible case in Section 6. We then compare the two cases in Section 7 and a show a discrepancy between them, which is further analyzed analytically in Section 8. Discussion (Section 9) and conclusion (Section 10) follow.

2. Model

We consider an elastic rod with a rectangular cross-section of width b and thickness h, total length L and arc length S in its unstressed reference state. In this state the rod lies along the $\boldsymbol{e_x}$ axis, from the origin $O=(0,0,0)$ to the point at $(L,0,0)$. The position vector of the center of the rod cross-section is noted $\boldsymbol{R}(S)$ and we have $\boldsymbol{R}(0)=(0,0,0)$ and $\boldsymbol{R}(L)=(L,0,0)$ in the reference state.

2.1. Kinematics

We use the special Cosserat theory of rods [10] where the rod can suffer bending, extension, and shear deformations. We work under the assumption that the rod cross-section remains planar (and rectangular) as the rod deforms and use a set of three Cosserat directors $(\boldsymbol{d_1}(S),\boldsymbol{d_2}(S),\boldsymbol{d_3}(S))$ embedded in each cross-section: $\boldsymbol{d_1}$ is perpendicular to the section plane, $\boldsymbol{d_2}$ is along the small span (of length h) of the section, and $\boldsymbol{d_3}$ is along the wide span (of length b) of the section. In the undeformed state, $\boldsymbol{d_1}(S)\equiv\boldsymbol{e_x}$, $\boldsymbol{d_2}(S)\equiv\boldsymbol{e_y}$, and $\boldsymbol{d_3}(S)\equiv\boldsymbol{e_z}$. We only consider deformed states that are (i) planar (where the rod centerline $\boldsymbol{R}(S)$ lies in the (x,y) plane, the rod being bent along its small span h) and (ii) twist-less (where the director $\boldsymbol{d_3}(S)\equiv\boldsymbol{e_z}$). Note that in the presence of extension and shear, S may no longer be the arc-length of the curve $\boldsymbol{R}(S)$ in the deformed state. We introduce extension and shear strains, e_1 and e_2, such that

$$\boldsymbol{R}'(S)\stackrel{\text{def}}{=}\mathrm{d}\boldsymbol{R}/\mathrm{d}S=(1+e_1)\boldsymbol{d_1}+e_2\boldsymbol{d_2}. \tag{1}$$

In the absence of extension ($e_1=0$) and shear ($e_2=0$), the director $\boldsymbol{d_1}$ is the unit tangent to the centerline $\boldsymbol{R}(S)=(X(S),Y(S),Z(S))$. We introduce the angle $\theta(S)$ to parametrize the rotation of the $(\boldsymbol{d_1},\boldsymbol{d_2})$ frame around the $\boldsymbol{e_z}=\boldsymbol{d_3}$ axis:

$$\boldsymbol{d_1}(S)=\begin{pmatrix}\cos\theta(S)\\ \sin\theta(S)\\ 0\end{pmatrix}_{\boldsymbol{e_x},\boldsymbol{e_y},\boldsymbol{e_z}} \quad\text{and}\quad \boldsymbol{d_2}(S)=\begin{pmatrix}-\sin\theta(S)\\ \cos\theta(S)\\ 0\end{pmatrix}_{\boldsymbol{e_x},\boldsymbol{e_y},\boldsymbol{e_z}}. \tag{2}$$

2.2. Dynamics

We use the Kirchhoff dynamical equations for elastic rods [10], where the stresses in the section are averaged to yield an internal force $\boldsymbol{N}(S)$ and an internal moment $\boldsymbol{M}(S)$. These internal forces and moments are the loads exerted on the section at S by the part of the rod at $\bar{S}>S$. In the absence of body force and couple, the linear and angular momentum balance then read

$$\boldsymbol{N}'(S,T)=\rho hb\ddot{\boldsymbol{R}}(S,T), \tag{3}$$

$$\boldsymbol{M}'(S,T)+\boldsymbol{R}'(S,T)\times\boldsymbol{N}(S,T)=\rho I\ddot{\theta}(S,T), \tag{4}$$

where $(\,)'\stackrel{\text{def}}{=}\partial/\partial S$, $\dot{(\,)}\stackrel{\text{def}}{=}\partial/\partial T$, T is time, ρ the mass per unit volume of the material, and I the second moment of area of the cross-section (in the present case $I=h^3b/12$).

2.3. Constitutive law

We use the standard linear constitutive relationship relating the bending strain $\kappa(S)\stackrel{\text{def}}{=}\theta'(S)$ to the bending moment $M_3\stackrel{\text{def}}{=}\boldsymbol{M}\cdot\boldsymbol{d_3}$:

$$M_3=EI\kappa, \tag{5}$$

where E is Young's modulus. Note that κ is not the curvature in general. In a similar way, the tension $N_1\stackrel{\text{def}}{=}\boldsymbol{N}\cdot\boldsymbol{d_1}$ and the shear force $N_2\stackrel{\text{def}}{=}\boldsymbol{N}\cdot\boldsymbol{d_2}$ are linked to the extension e_1 and shear strains e_2 through

$$N_1=Ehbe_1, \tag{6}$$

$$N_2 = Ghbe_2, \tag{7}$$

where G is the shear modulus.

2.4. Equations in component form

In the planar case considered here, we have $Z(S,T)\equiv 0$, $N_z(S,T)\equiv 0$, $M_x(S,T)\equiv 0$, and $M_y(S,T)\equiv 0$, $\forall(S,T)$ so that the equations for the six remaining unknowns are

$$X' = (1+e_1)\cos\theta - e_2\sin\theta, \tag{8a}$$

$$Y' = (1+e_1)\sin\theta + e_2\cos\theta, \tag{8b}$$

$$\theta' = M/(EI), \tag{8c}$$

$$M' = e_2N_1 - (1+e_1)N_2 + \rho I\ddot{\theta}, \tag{8d}$$

$$N_x' = \rho hb\ddot{X}, \tag{8e}$$

$$N_y' = \rho hb\ddot{Y}, \tag{8f}$$

where $M = M_z = M_3$, $N_1 = N_x\cos\theta + N_y\sin\theta$, and $N_2 = -N_x\sin\theta + N_y\cos\theta$. The strains (e_1,e_2) are given by Eqs. (6) and (7) as functions of N_x and N_y.

2.5. Dimensionless variables

We scale all lengths with L, time with $\tau \stackrel{\text{def}}{=} L^2\sqrt{\rho hb/(EI)}$, forces with EI/L^2, and moments with EI/L. This naturally introduces a parameter

$$\eta \stackrel{\text{def}}{=} \frac{I}{hbL^2} = \frac{1}{12}\left(\frac{h}{L}\right)^2, \tag{9}$$

which takes small values in the present case of slender rods. Dimensionless variables will be written lowercase, e.g. $x \stackrel{\text{def}}{=} X/L$, or $m \stackrel{\text{def}}{=} ML/(EI)$. The constitutive relations (6) and (7) read: $e_1 = \eta n_1$ and $e_2 = 2(1+\nu)\eta n_2$, where the Poisson ratio ν arises from the relation $E = 2(1+\nu)G$. Rods with $\eta > 0$ are extensible, shearable rods for which the rotational inertia is accounted for. They will be simply called *extensible* rods. Rods with $\eta = 0$ will be simply called *inextensible* rods, although they really are inextensible, unshearable rods for which the rotational inertia is ignored. Such rods are frequently called elastica [16,17].

3. Small-amplitude vibrations around pre- and post-buckled equilibrium

The systems of (8) in dimensionless form reads

$$x'(s,t) = \cos\theta + \eta(n_1\cos\theta - 2(1+\nu)n_2\sin\theta), \tag{10a}$$

$$y'(s,t) = \sin\theta + \eta(n_1\sin\theta + 2(1+\nu)n_2\cos\theta), \tag{10b}$$

$$\theta'(s,t) = m, \tag{10c}$$

$$m'(s,t) = -n_2 + \eta((1+2\nu)n_1n_2 + \ddot{\theta}), \tag{10d}$$

$$n_x'(s,t) = \ddot{x}, \tag{10e}$$

$$n_y'(s,t) = \ddot{y}, \tag{10f}$$

with $n_1 = n_x\cos\theta + n_y\sin\theta$ and $n_2 = -n_x\sin\theta + n_y\cos\theta$. In our problem, we consider a clamped–clamped rod and control the end-shortening $d \stackrel{\text{def}}{=} 1-(x(1,t)-x(0,t))$. This setup implies the following boundary conditions:

$$x(0,t) = 0, \quad x(1,t) = 1-d, \tag{11a}$$

$$y(0,t) = 0, \quad y(1,t) = 0, \tag{11b}$$

$$\theta(0,t) = 0, \quad \theta(1,t) = 0. \tag{11c}$$

For each given value of the end-shortening d, we find the equilibrium configuration $(x_e, y_e, \theta_e, m_e, n_{xe}, n_{ye})$ by solving system (10) with $\ddot{x}_e = 0$ and $\ddot{y}_e = 0$. Then we look for small-amplitude vibrations around this equilibrium configuration,

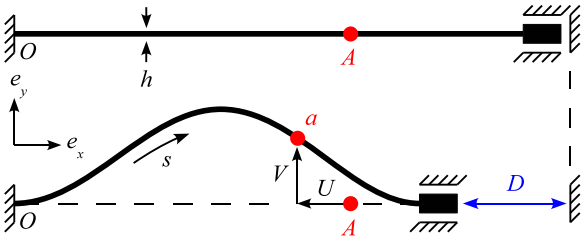

Fig. 1. Clamped–clamped rod buckled in the (x,y) plane. The end-shortening D is controlled. The point A in the reference configuration moves to point a in the deformed configuration, introducing horizontal $U \leq 0$ and vertical V displacements. The origin is taken at the fixed point O at the left end of the rod.

that is, we set

$$x(s,t) = x_e(s) + \delta \overline{x}(s) e^{\imath\omega t}, \tag{12a}$$

$$y(s,t) = y_e(s) + \delta \overline{y}(s) e^{\imath\omega t}, \tag{12b}$$

$$\theta(s,t) = \theta_e(s) + \delta \overline{\theta}(s) e^{\imath\omega t}, \tag{12c}$$

$$m(s,t) = m_e(s) + \delta \overline{m}(s) e^{\imath\omega t}, \tag{12d}$$

$$n_x(s,t) = n_{xe}(s) + \delta \overline{n}_x(s) e^{\imath\omega t}, \tag{12e}$$

$$n_y(s,t) = n_{ye}(s) + \delta \overline{n}_y(s) e^{\imath\omega t}, \tag{12f}$$

where $\delta \ll 1$ is a small parameter, and ω is the frequency of the vibration. Inserting (12) into (10) and keeping only linear terms in δ, we obtain equations for the spatial modes $(\overline{x},\overline{y},\overline{\theta},\overline{m},\overline{n}_x,\overline{n}_y)$:

$$\overline{x}'(s) = -\overline{\theta}\ \sin\theta_e + \eta(\overline{n}_1 \cos\theta_e - 2(1+\nu)\overline{n}_2 \sin\theta_e) + \eta\overline{\theta}(-n_{1e}\sin\theta_e - 2(1+\nu)n_{2e}\cos\theta_e), \tag{13a}$$

$$\overline{y}'(s) = \overline{\theta}\cos\theta_e + \eta(\overline{n}_1 \sin\theta_e + 2(1+\nu)\overline{n}_2 \cos\theta_e) + \eta\overline{\theta}(n_{1e}\cos\theta_e - 2(1+\nu)n_{2e}\sin\theta_e), \tag{13b}$$

$$\overline{\theta}'(s) = \overline{m}, \tag{13c}$$

$$\overline{m}'(s) = -\overline{n}_2 + \eta((1+2\nu)(\overline{n}_1\, n_{2e} + n_{1e}\overline{n}_2) - \omega^2\overline{\theta}), \tag{13d}$$

$$\overline{n}_x'(s) = -\omega^2\overline{x}, \tag{13e}$$

$$\overline{n}_y'(s) = -\omega^2\overline{y}, \tag{13f}$$

with $\overline{n}_1 = \overline{n}_x\cos\theta_e + \overline{n}_y\sin\theta_e + \overline{\theta}(-n_{xe}\sin\theta_e + n_{ye}\cos\theta_e)$ and $\overline{n}_2 = -\overline{n}_x\sin\theta_e + \overline{n}_y\cos\theta_e + \overline{\theta}(-n_{xe}\cos\theta_e - n_{ye}\sin\theta_e)$. The boundary conditions on the spatial modes are

$$\overline{x}(0) = 0, \quad \overline{x}(1) = 0, \tag{14a}$$

$$\overline{y}(0) = 0, \quad \overline{y}(1) = 0, \tag{14b}$$

$$\overline{\theta}(0) = 0, \quad \overline{\theta}(1) = 0. \tag{14c}$$

For given parameters η and ν and given end-shortening d, the equilibrium $(x_e,y_e,\theta_e,m_e,n_{xe},n_{ye})$ is first computed from (10) with $\ddot{x}_e = 0$ and $\ddot{y}_e = 0$. Then the 6D system (13) with the six boundary conditions (14) is a well-defined boundary value problem, but with the additional unknown ω. For computational purpose, we normalize the linear solution of this problem by imposing the condition

$$\overline{m}^2(0) + \overline{n}_x^2(0) + \overline{n}_y^2(0) = 1. \tag{15}$$

4. Equilibrium

We use a 'home-made' predictor–corrector path-following code to address the problem numerically. For each value of $p \stackrel{\text{def}}{=} -n_{xe} = -N_{xe}L^2/(EI)$ in the interval $(0; 8\pi^2)$, we compute the equilibrium solution $(x_e,y_e,\theta_e,m_e,n_{xe},n_{ye})$ satisfying clamped–clamped boundary conditions (11).

In Fig. 2 equilibrium paths are given for both inextensible (i.e. $\eta = 0$) and extensible ($\eta > 0$) rods. In the latter case, we see that the displacement d starts to increase as soon the curve leaves the origin: due to extensibility the rod shorten before buckling. Buckling happens at $p = 4\pi^2$ for the inextensible case and at lower values for extensible cases. These

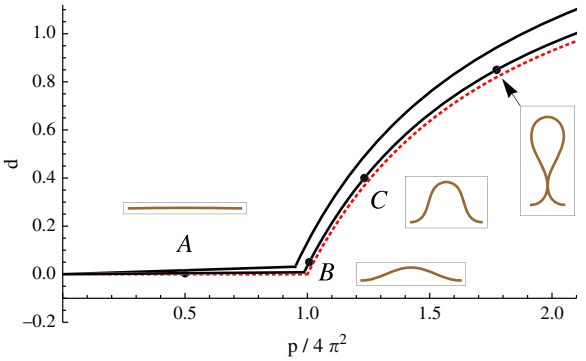

Fig. 2. Fundamental and post-buckled equilibrium path of a clamped–clamped rod with $\eta = 1/1200$, $\eta = 1/4800$, and $\eta = 0$ (top to bottom). As the controlled end-shortening $d = D/L$ is gradually raised, an increasing axial load $p = -N_{xe}L^2/(EI)$ is recorded. (For interpretation of the references to color in this figure legend, the reader is referred to the web version of this article.)

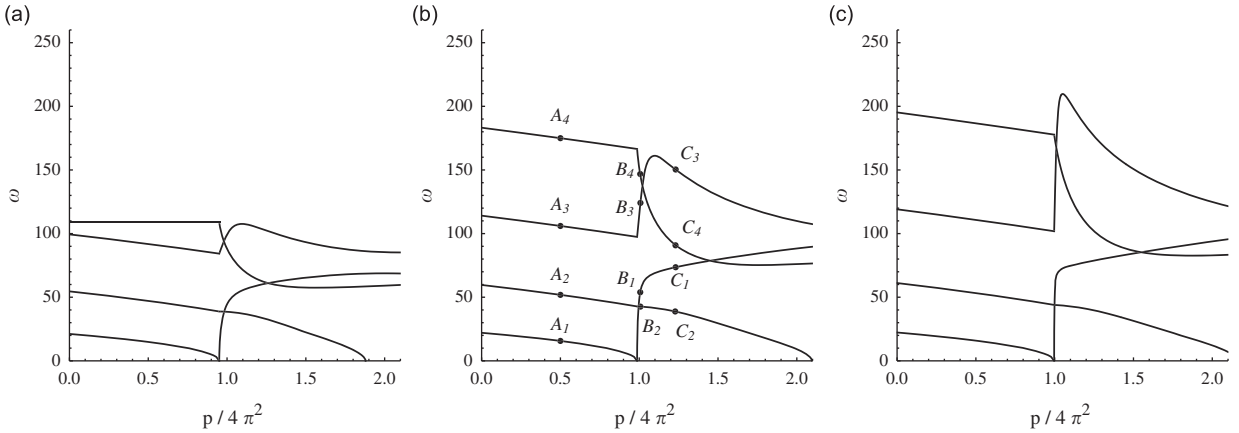

Fig. 3. Frequencies for the lowest four vibration modes of a clamped–clamped rod around its fundamental and post-buckled equilibrium configurations in the extensible case: (a) for $\eta = 1/1200$, (b) for $\eta = 1/4800$, (c) for $\eta = 1/19\,200$ (plain). The labels A_i, B_i, C_i with $i = 1,2,3,4$ correspond to the shapes given in Figs. 4–6.

equilibrium paths show that extension and shear play a minor role in the buckling load and that the inextensible rod solution is obtained in the limit $\eta \to 0$ of the extensible rod solution, as expected. Closed-form formula for the dotted (red) curve is given in Appendix A.

5. Vibrations in the extensible case

5.1. Vibrations around the straight state

We first consider the equilibrium solution where the axially loaded rod is straight, but compressed:

$$y_e(s) = 0, \quad x_e(s) = (1-\eta p)s, \quad n_{ye}(s) = 0, \quad n_{xe}(s) = -p, \quad \theta_e(s) = 0, \quad m_e(s) = 0. \tag{16}$$

The vibrations around this straight equilibrium are either extensional of flexural. Extensional vibrations modes are solutions of

$$\overline{x}'(s) = \eta \overline{n}_x, \tag{17a}$$

$$\overline{n}_x'(s) = -\omega^2 \overline{x}, \tag{17b}$$

with boundary conditions $\overline{x}(0) = 0 = \overline{x}(1)$. This yields vibration frequencies of the form $\omega = j\pi/\sqrt{\eta}$ (with $j = 1,2,\ldots$), which do not vary with the load p. The upper curve, before buckling of Fig. 3(a) is such a solution. Flexural vibrations modes are solutions of

$$\overline{y}'''' + \mu_p \overline{y}'' - \mu_\omega^2 \overline{y} = 0, \tag{18}$$

with boundary conditions $\overline{y}(0) = 0 = \overline{y}(1)$ and $(\eta_\star^2\omega^2 + [1-p(\eta-\eta_\star)]^2)\overline{y}'(0,1) + \eta_\star \overline{y}'''(0,1) = 0$. We introduced the notations $\eta_\star = 2\eta(1+\nu)$, $\mu_p = (1-p(\eta-\eta_\star))p + \omega^2(\eta+\eta_\star)$, and $\mu_\omega^2 = \omega^2([1-p(\eta-\eta_\star)]^2 - [1-p(\eta-\eta_\star)]p\eta_\star - \eta\eta_\star\omega^2)$. The general solution is

of the form

$$\overline{y}(s) = A\cos k^+ s + B\cosh k^- s + C\sin k^+ s + D\sinh k^- s, \tag{19}$$

where we used the two wavenumbers $k^\pm = (1/\sqrt{2})\sqrt{\sqrt{\mu_p^2+4\mu_\omega^2} \pm \mu_p}$. The boundary conditions require that

$$2a^+a^-k^+k^-(\cos k^+\cosh k^- - 1) + ((a^+k^+)^2 - (a^-k^-)^2)\sin k^+\sinh k^- = 0, \tag{20}$$

with $a^\pm = [1-p(\eta-\eta_\star)]^2 + \eta_\star(\mp(k^\pm)^2 + \eta_\star\omega^2)$, which is an equation for ω. The analytical solutions $\omega(p)$ given by (20) match numerical solutions given in Fig. 3(a)–(c). Buckling occurs when $\omega = 0 = \mu_\omega$, i.e. for $k^+ = \sqrt{\mu_p} = 2\pi$ and $k^- = 0$. This yields

$$p = \frac{\sqrt{1+16\pi^2(\eta_\star-\eta)}-1}{2(\eta_\star-\eta)} = 4\pi^2 - 16\pi^4(\eta_\star-\eta) + O(\eta^2). \tag{21}$$

5.2. Vibrations around the buckled state

Once the equilibrium solution is known, we solve the boundary value problem (13)–(14) numerically with a shooting method: (i) we first use a guess for the unknown parameters $\chi = (\overline{m}(0), \overline{n}_x(0), \overline{n}_y(0), \omega)$ and we integrate the system (13) up to $s=1$; (ii) we then check if the boundary conditions (14)–(15) are satisfied. If not, we change the guess χ accordingly (using a Newton–Raphson scheme) until the boundary conditions at $s=1$ are satisfied.

Once a solution χ_i is found for a given $p = p_i$, we set $p = p_{i+1}$ and use the value χ_i as starting guess (predictor step) for the shooting method at $p = p_{i+1}$ (corrector step). In this setup, each curve $\omega = \omega(p)$ represents a path in the numerical bifurcation diagram, and we have numerically computed the four first paths (i.e. lowest four curves $\omega = \omega(p)$) for several values of the parameter $\eta = I/(hwL^2)$.

In Fig. 3, frequencies for the first four modes are given as a function of the parameter p, for different values of η. It should be noted that the computations performed here are for a displacement control experiment, that is d (and not p) is controlled. Nevertheless, as there is a one-to-one correspondence between d and p, for each value of the applied longitudinal displacement d, the equilibrium axial load p is read from Fig. 2 and then the frequency is computed and plotted in Fig. 3. We see in Fig. 3 that as $\eta \to 0$, frequencies globally increase and tend toward limiting curves. Finally we note that every curve $\omega(p)$ is continuous, but that the curves for the odd modes experience a rapid increase just after buckling. As $\eta \to 0$ this rapid increase becomes more abrupt to eventually turn into a discontinuity in the case $\eta = 0$, see Section 6. In each of Figs. 4–6, dynamical shapes ($x(s,t) = x_e(s) + \overline{x}(s)\cos\omega t$, $y(s,t) = y_e(s) + \overline{y}(s)\cos\omega t$) of the vibrating rod are plotted.

We now focus on the first mode, which emerges from $\omega = 0$ at buckling. In Fig. 7(a), we plot ω as function of the rise of the buckled rod at its mid-point: $y_e(1/2) = Y_e(L/2)/L$. Each curve corresponds to a different value of the parameter η, from $\eta = 1/1200$ (i.e. $L = 10h$) to $\eta = 1/480\,000$ (i.e. $L = 200h$). We see that all curves emerge from $\omega = 0$ at buckling ($y_e(1/2) = 0$) and asymptotically tend to the curve computed in the inextensible case (see Section 6) when $y_e(1/2)$ becomes large. For very small η values, curves rise sharply from $\omega = 0$ and quickly approaches the inextensible asymptote.

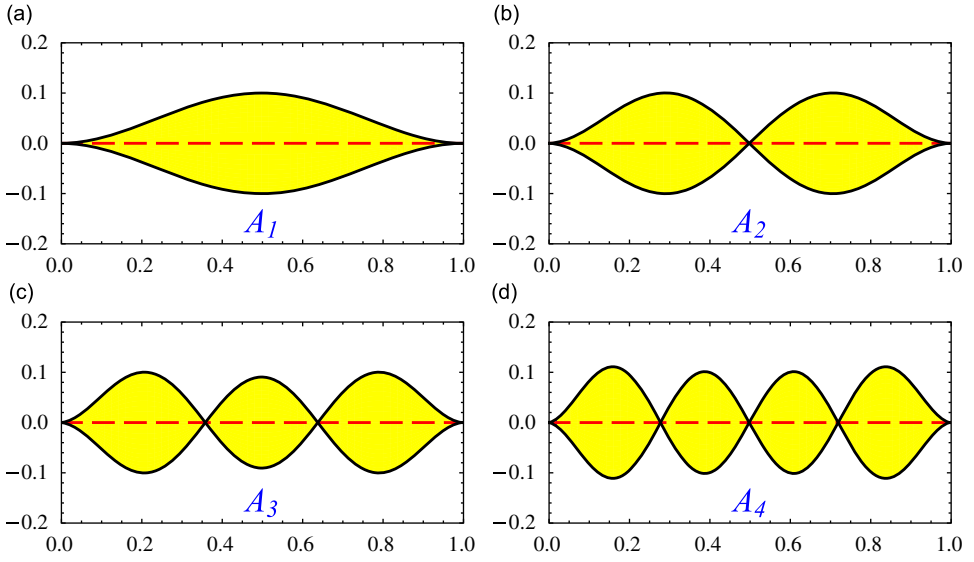

Fig. 4. First four modes at $p/(4\pi^2) = 0.5$, for the extensible case with $\eta = 1/4800$: configurations A_1 (a), A_2 (b), A_3 (c), and A_4 (d) in Fig. 3(b).

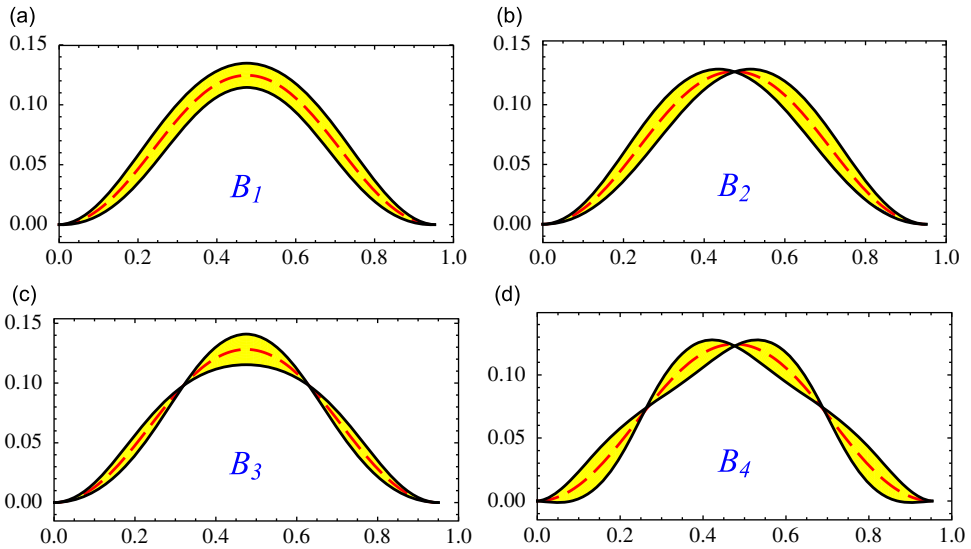

Fig. 5. First four modes at $d=0.05$, for $\eta = 1/4800$: configurations D_1 (a), D_2 (b), D_3 (c), and D_4 (d) in Fig. 3.

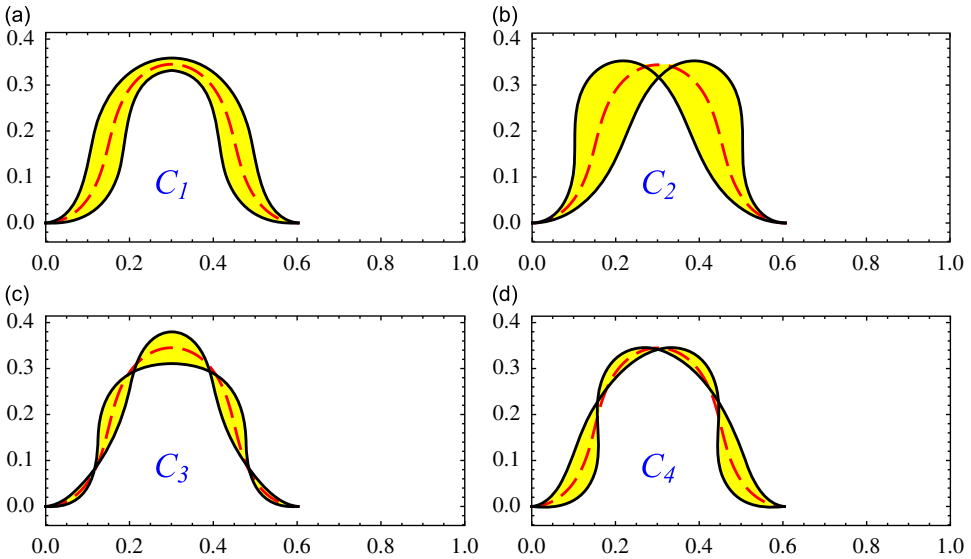

Fig. 6. First four modes at $d=0.4$, for $\eta = 1/4800$: configurations E_1 (a), E_2 (b), E_3 (c), and E_4 (d) in Fig. 3.

As a matter of fact these curves can be made to almost collapse on a master curve if the horizontal axis is plotted in unit of the rod thickness h: in Fig. 7(b) we plot the frequency ω as function of $Y_e(L/2)/h$, for the same set of η values. All curves nearly collapse on a master curve which has a (numerically determined) slope $\simeq 28$ at the origin. Using $h=\sqrt{12\eta}L$ we obtain

$$\omega \simeq \frac{8.1}{\sqrt{\eta}}\frac{Y_e(1/2)}{L}, \tag{22}$$

which means that the limit $\eta \to 0$ is singular for this first mode. The same phenomenon happens for all odd modes.

In dimensional form (i.e. $\Omega = \omega\sqrt{EI/(\rho h b)}/L^2$) we have the following expression for the frequency Ω (in rad/s):

$$\Omega \simeq 8.1\frac{Y_e(L/2)}{L^2}\sqrt{\frac{E}{\rho}} \quad \text{for } Y_e(L/2) \lesssim 2h. \tag{23}$$

The presence of the celerity $c=\sqrt{E/\rho}$ of compression elastic waves in this expression shows that directly after buckling and for a short loading interval (i.e. $Y_e(L/2)=0$ to $Y_e(L/2)\simeq 2h$), the lowest mode of vibration of a buckled rod is of extension–compression type. We also see in Fig. 7(b) that for $Y_e(L/2) \gtrsim 8h$ the behavior is of flexural type (i.e. curves have reached the inextensible asymptote). This separation between two different behaviors in the elastic response of the rod

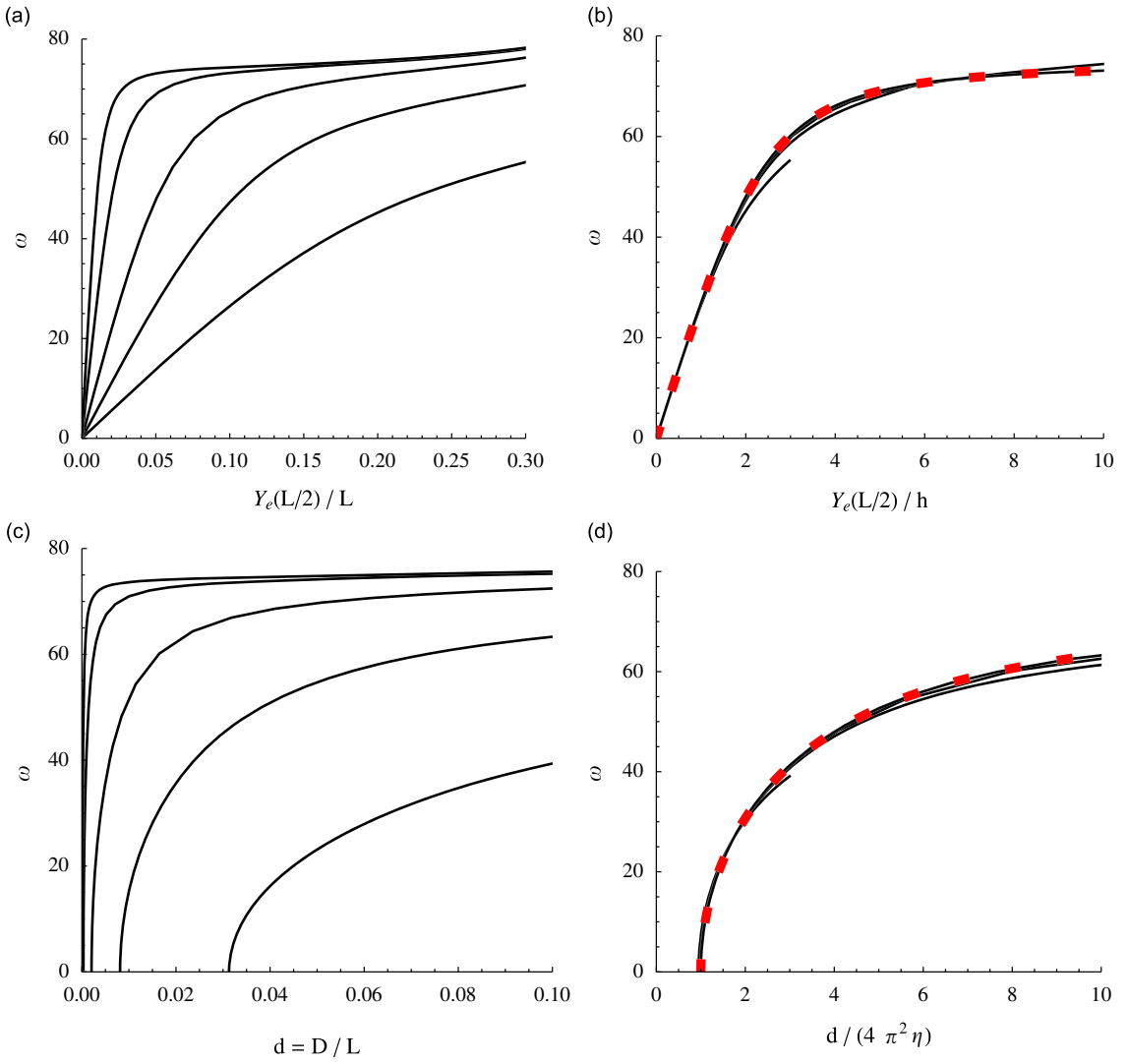

Fig. 7. Post-buckled frequency of the mode emerging from $\omega = 0$ at buckling (for $\eta > 0$). (a) From bottom to top: $1/\eta = 1200, 4800, 19\,200, 120\,000, 480\,000$. (b) Same data but with horizontal axis rescaled with h. The curves nearly collapse on a master curve whose slope at the origin is $\simeq 28$. The dashed curve (red online), whose slope at the origin is $2\sqrt{2}\pi^2 \simeq 27.9$ and which is hardly distinguishable from the previous ones, is the first mode solution of (25). (c) Same data as in (a) but with $d = D/L$ on the horizontal axis. (d) Same data but with the horizontal axis rescaled with $(4\pi^2\eta)$; as in (b) the curves nearly collapse on a master curve. The dashed curve (red online), which is hardly distinguishable from the previous ones, is the first mode solution of (25). (For interpretation of the references to color in this figure legend, the reader is referred to the web version of this article.)

could be a way to define the notion of a shallow (resp. deep) buckled equilibrium shape: a shallow (resp. deep) equilibrium shape has a vibrational response that is primarily extensional (resp. flexural).

We now focus on the second mode and show that it does not suffer the same singularity as the first one. The mode frequency emerges from a finite value $\omega_b = \omega_b(\eta)$ at buckling, and we see in Fig. 3 that its variation (with p) after buckling is much slower than for the first mode. In Fig. 8 the variation of the second mode frequency is plotted as a function of $y_e(1/2) = Y_e(L/2)/L$. We numerically extract the approximation:

$$\omega \simeq \omega_b(\eta) - (9 - 5400\eta)\left(\frac{Y_e(L/2)}{L}\right)^2. \tag{24}$$

In conclusion, the limit $\eta \to 0$ is smooth for the second mode (and in fact for all even modes).

An alternative equation is used in (for example) [12–15] for the vibrations of post-buckled extensible rods. The transverse displacement $Y(S,T)$ is the solution of the equation:

$$EIY'''' + \rho hb\ddot{Y} + PY'' = 0, \tag{25a}$$

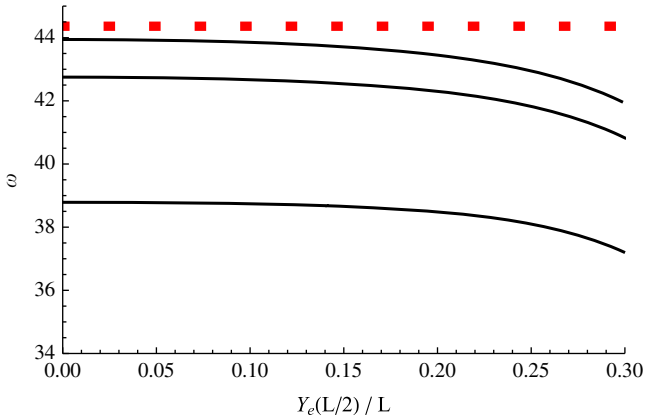

Fig. 8. Post-buckled frequency of the second mode (for $\eta > 0$). Continuous (black) curves are, from bottom to top, for $1/\eta = 1200, 4800, 19\,200$. The (red) dashed curve is the second mode solution of (25). (For interpretation of the references to color in this figure legend, the reader is referred to the web version of this article.)

$$\text{with} \quad P = \frac{Ehb}{L}\left(D - \frac{1}{2}\int_0^L Y'^2 \, \mathrm{d}S\right). \tag{25b}$$

In this model a certain number of assumptions on the nonlinear terms are made, see e.g. Eq. (B.3). Calculating the frequency of the first mode just after buckling, we find

$$\Omega \simeq \sqrt{2/3}\pi^2 \frac{Y_e(L/2)}{L^2}\sqrt{\frac{E}{\rho}}, \tag{26}$$

where $\sqrt{2/3}\pi^2 \simeq 8.06$, in agreement with our result (23). We plot in Fig. 7(b) and (d) the first mode solution of Eq. (25), and we note that this solution is independent of η, which is not the case for Kirchhoff equations. Moreover the second mode of (25) is found to be independent of $Y_e(L/2)$ (see Fig. 8), in contradiction with (24). A more comprehensive comparison of the two models is the subject of a forthcoming paper.

6. Vibrations in the inextensible case

6.1. Vibrations around the straight state

We consider an inextensible unshearable rod of length L, strongly held at both sides by clamps separated by a distance L. The rod is held straight and hence no flexural dynamics at all can take place, i.e. flexural vibrations (that would be given by the $\eta = 0$ version of Eq. (18)) are impossible here as they would require shortening of the ends.

Axial vibrations are given by

$$\overline{x}'(s) = 0, \tag{27a}$$

$$\overline{n}_x'(s) = -\omega^2 \overline{x}, \tag{27b}$$

with boundary conditions $\overline{x}(0) = 0 = \overline{x}(1)$. The solution is $\overline{x}(s) \equiv 0$, and $\overline{n}_x(s) \equiv$ constant, where we see that any ω is admissible. Even if no extensional deformation is present, the load in this statically indeterminate problem can fluctuate with any frequency. This is illustrated in Fig. 9 by the (red) shaded region in the interval $0 \le p \le 4\pi^2$.

6.2. Vibrations around the buckled state

As in the extensible case we solve the boundary value problem (13)–(14) numerically with a shooting method. The results are shown in Fig. 9 and in particular we see that at the buckling threshold, the first four frequencies are: $\omega \simeq 44.36$, 74.4, 182.1, and 259.4. Only one out of two of these frequencies is close to what was found in Fig. 3(c).

Dynamical shapes $(x(s,t) = x_e(s) + \overline{x}(s)\cos\omega t,\ y(s,t) = y_e(s) + \overline{y}(s)\cos\omega t)$ of the vibrating rod are plotted in Figs. 10 and 11.

7. Comparison of the extensible and inextensible results

We here compare the post-buckled vibrations frequencies obtained numerically for the extensible ($\eta > 0$) and inextensible ($\eta = 0$) cases. On the one hand, we see in Fig. 9 that in the inextensible case there is no curve emerging from $\omega = 0$ at buckling, whereas there is always one for all η values in the extensible case (Fig. 3). On the other hand, in the

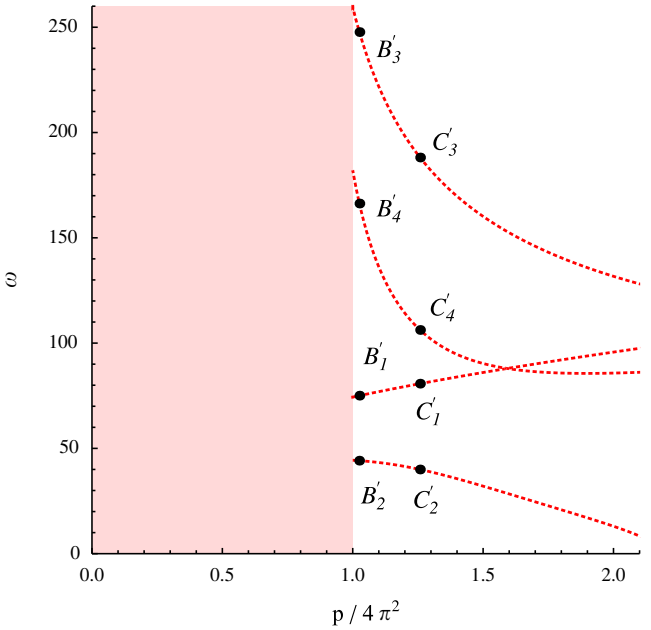

Fig. 9. Frequencies for the lowest four vibration modes of a clamped–clamped rod around its fundamental and post-buckled equilibrium configurations in the inextensible case $\eta = 0$. The labels B_i', C_i' with $i = 1, 2, 3, 4$ correspond to the shapes given in Figs. 10 and 11. (For interpretation of the references to color in this figure legend, the reader is referred to the web version of this article.)

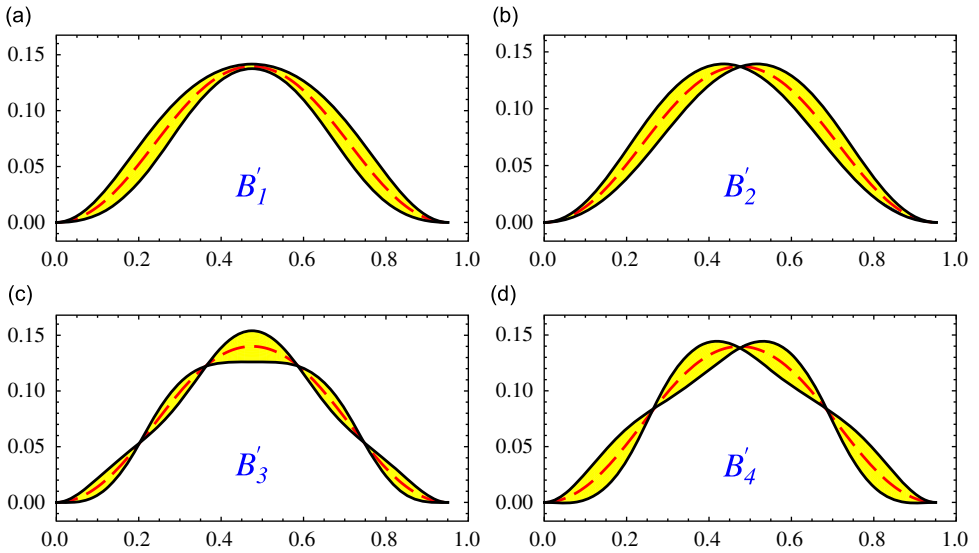

Fig. 10. First four modes at $d = 0.05$, in the inextensional case: configurations B_1 (a), B_2 (b), B_3 (c), and B_4 (d) in Fig. 3.

inextensible case there is a curve emerging from $\omega \simeq 74.4$, nowhere near any of the extensible curves. We plot in Fig. 12(a) a comparison of the inextensible $\eta = 0$ and extensible $\eta = 1/19\,200$ cases, for the first two modes. We see that the second extensible mode (emerging from $\omega \simeq 44$ at buckling) is always very close to its inextensible counterpart, but that the first extensible mode (emerging from $\omega = 0$ at buckling) is first very far from its inextensible counterpart and only approaches it later in the post-buckling regime. The consequence is that for a short interval after buckling the inextensible model wrongly predicts a fundamental mode at $\omega \simeq 44$ whereas for any 'real life' elastic rod there is a vibration mode with lower frequency.

A full comparison between extensible and inextensible cases shows that all extensible odd modes experiences a similar mismatch with their inextensible counterpart, see Fig. 12(b) for the first four modes. For the solution at buckling, with p given by (21), we further investigate numerically the variation with η of the frequencies of the first four modes in the

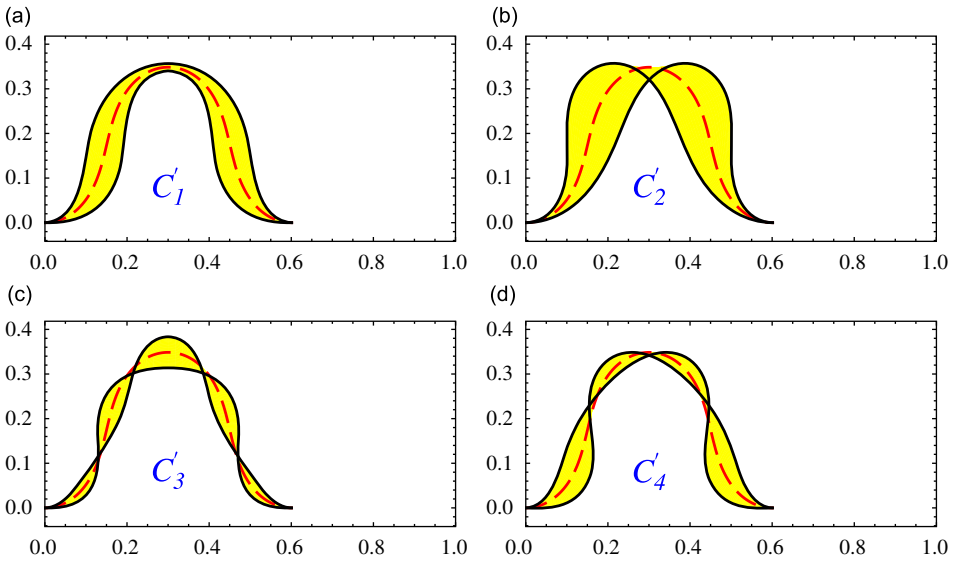

Fig. 11. First four modes at $d=0.4$, in the inextensional case: configurations C_1 (a), C_2 (b), C_3 (c), and C_4 (d) in Fig. 3.

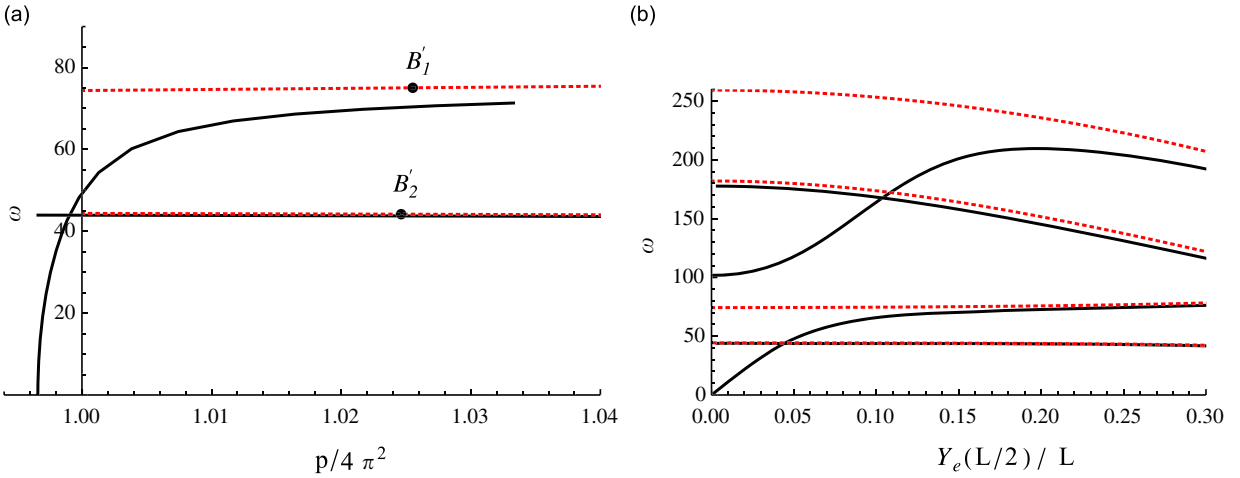

Fig. 12. Frequencies of a clamped–clamped rod around its post-buckled equilibrium configurations. Comparison of the extensible case ($\eta = 1/19\,200$, plain curve) with the inextensible case (dotted, red) (a) for lowest two vibration modes, and (b) for lowest four vibration modes and plotted as a function of $Y_e(L/2)$, the rise of the buckled equilibrium shape at its middle point. (For interpretation of the references to color in this figure legend, the reader is referred to the web version of this article.)

extensible case and compare them with the first four frequency of the inextensible case $\eta = 0$. In Fig. 13, we see that as $\eta \to 0$ the even extensible modes are converging to solutions of the inextensible case, but that the limit $\eta \to 0$ of the odd extensible modes does not correspond to the frequency values found in the inextensible case.

8. Analytical study for the inextensible case

In order to understand the mismatch of the odd modes' frequencies at buckling between the extensible and inextensible cases, we look at the problem analytically. In the inextensible case, buckling happens for $p = 4\pi^2$. We look for the frequencies that emerge from the continuum present for $p \leq 4\pi^2$. If the $\eta \to 0$ limit was not singular we would just look for the solutions of (20) for $\eta = 0$ and $p = 4\pi^2$, that is

$$2k^+k^-(\cos k^+ \cosh k^- - 1) + 4\pi^2 \sin k^+ \sinh k^-, \tag{28}$$

with $k^\pm = \sqrt{\sqrt{4\pi^4+\omega^2} \pm 2\pi^2}$. The solutions are listed in Table 1 and we see that, for the odd modes, they do not match what is found numerically.

To investigate matter further we set $\eta = 0$ in (10), and look for the frequency values that exist just after buckling (i.e. around post-buckled configurations). In the post-buckled configuration, the equilibrium equations and the boundary

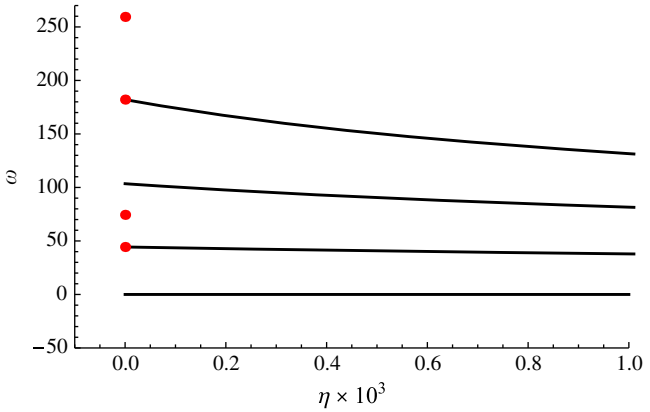

Fig. 13. The curves show the variation with η of the frequencies of the first four modes in the extensible case, at the buckling threshold. The (red) dots at $\eta=0$ show the frequency values of the first four modes of the inextensible case, at the buckling threshold. A mismatch for half of the modes exists. (For interpretation of the references to color in this figure legend, the reader is referred to the web version of this article.)

Table 1
Frequencies and wavenumbers for the lowest eight modes of vibration as given by Eq. (20) for $p=4\pi^2$ and $\eta=0$. This also corresponds to the first eight solutions of $P_1(\omega_0)=0$ (see Eq. (38)).

i	1	2	3	4	5	6	7	8
ω	0	44.36	103.5	182.1	280.6	398.8	536.8	694.6
k^+	2π	8.26	11.18	14.25	17.35	20.5	23.6	26.7
$(k^+ \bmod 2\pi)/(\pi/2)$		1.26	3.12	1.07	3.04	1.03	3.02	1.02
k^-	0	5.37	9.25	12.8	16.2	19.5	22.7	25.98

conditions are given by

$$n_{ye}=const, \tag{29a}$$

$$n_{xe}=-p, \tag{29b}$$

$$\theta_e''=-p\sin\theta_e-n_{ye}\cos\theta_e \quad \text{with } \theta_e(0)=0=\theta_e(1), \tag{29c}$$

$$x_e'=\cos\theta_e \quad \text{with } x_e(1)-x_e(0)=1-d, \tag{29d}$$

$$y_e'=\sin\theta_e \quad \text{with } y_e(0)=y_e(1) \tag{29e}$$

and without loss of generality, we choose $x_e(0)=y_e(0)=0$. For equilibrium modes whose shapes are invariant when reflected along the line parallel to the $\boldsymbol{e_y}$ axis and containing the point $(x(1/2),0)$, we have $n_{ye}=\text{constant}=0$ in Eq. (29a). The first bifurcated equilibrium mode, represented in Fig. 1 we focus, is such a mode. We address the behavior of the solutions after but close to buckling. Therefore, we expand the variables $\theta_e(s)$ and $y_e(s)$ in powers of ε, a small parameter measuring the distance from buckling:

$$\theta_e(s)=\varepsilon\theta_1(s)+\varepsilon^2\theta_2(s)+\varepsilon^3\theta_3(s)+O(\varepsilon^4), \tag{30a}$$

$$x_e(s)=\varepsilon x_1(s)+\varepsilon^2 x_2(s)+\varepsilon^3 x_3(s)+O(\varepsilon^4), \tag{30b}$$

$$y_e(s)=\varepsilon y_1(s)+\varepsilon^2 y_2(s)+\varepsilon^3 y_3(s)+O(\varepsilon^4), \tag{30c}$$

$$p=p_0+\varepsilon p_1+\varepsilon^2 p_2+\varepsilon^3 p_3+O(\varepsilon^4). \tag{30d}$$

We substitute these expansions in the equilibrium equations (29), which have to be satisfied to all orders in ε. The solution up to order 3 reads:

$$\theta_e(s)=\varepsilon\sin 2\pi s+\frac{\varepsilon^3}{48}\cos^2(2\pi s)\sin(2\pi s)+O(\varepsilon^4), \tag{31a}$$

$$x_e(s)=s+\frac{\varepsilon^2}{16\pi}(\sin 4\pi s-4\pi s)+O(\varepsilon^4), \tag{31b}$$

$$y_e(s) = \frac{\varepsilon}{2\pi}(1-\cos 2\pi s) + \frac{\varepsilon^3}{384\pi}(-20+23\cos(2\pi s)-3\cos(6\pi s)) + O(\varepsilon^4), \tag{31c}$$

$$p = 4\pi^2 + \varepsilon^2\pi^2/2 + O(\varepsilon^4). \tag{31d}$$

In order to relate ε to the control parameter d and the amplitude after bifurcation, we compute the end-shortening

$$d = 1-(x_e(1)-x_e(0)) = \varepsilon^2/4 + O(\varepsilon^4) = 2\left(\frac{p}{4\pi^2}-1\right) + O(\varepsilon^4) \tag{32}$$

and the rod maximum deflection

$$y_e(1/2) = \frac{\varepsilon}{\pi}\left(1-\frac{5}{48}\varepsilon^2\right) + O(\varepsilon^4). \tag{33}$$

8.1. Vibration around the post-buckled equilibrium

We expand all modal variables $(\overline{x},\overline{y},\overline{\theta},\overline{m},\overline{n}_x,\overline{n}_y)$ and the frequency ω in powers of ε. For instance, we have $\omega = \omega_0 + \varepsilon\omega_1 + \varepsilon^2\omega_2 + \varepsilon^3\omega_3 + O(\varepsilon^4)$, and so on. We can now solve Eqs. (13) (with $\eta = 0$) with boundary conditions (14), using the equilibrium solution (31). To order ε^0 we have

$$\overline{x}_0' = 0 \quad \text{with } \overline{x}_0(0) = 0 = \overline{x}_0(1), \tag{34a}$$

$$\overline{n}_{x0}' = -\omega_0^2\overline{x}_0, \tag{34b}$$

$$\overline{y}_0'''' + 4\pi^2\overline{y}_0'' - \omega_0^2\overline{y}_0 = 0 \quad \text{with} \quad \overline{y}_0(0) = \overline{y}_0(1) = \overline{y}_0'(0) = \overline{y}_0'(1) = 0. \tag{34c}$$

The first two equations describe the longitudinal mode and are decoupled from the third one which is associated with the transverse mode. More precisely, the longitudinal mode is given by

$$\overline{x}_0(s) = 0 \quad \text{and} \quad \overline{n}_{x0}(s) \text{ constant}, \tag{35}$$

whereas for the transverse mode, the solution $\overline{y}_0(s)$ is

$$\overline{y}_0(s) = A_0\left(\frac{\cos k_0^+ s - \cosh k_0^- s}{\cos k_0^+ - \cosh k_0^-} - \frac{k_0^-\sin k_0^+ s - k_0^+\sinh k_0^- s}{k_0^-\sin k_0^+ - k_0^+\sinh k_0^-}\right), \tag{36}$$

with $k_0^\pm \overset{\text{def}}{=} \sqrt{\sqrt{4\pi^4+\omega_0^2} \pm 2\pi^2}$. The boundary conditions impose that

$$A_0 P_1(\omega_0) = 0, \tag{37}$$

with

$$P_1(\omega_0) \overset{\text{def}}{=} 2k_0^+ k_0^-(\cos k_0^+ \cosh k_0^- - 1) + 4\pi^2 \sin k_0^+ \sinh k_0^-, \tag{38}$$

which is an equation for ω_0. The first eight solutions of $P_1(\omega_0) = 0$ are listed in Table 1. Note that to order ε^0 there is no frequency jump. To order ε^1 we have

$$\overline{x}_1' = \overline{\theta}_0 \sin 2\pi s \quad \text{with } \overline{x}_1(0) = 0 = \overline{x}_1(1), \tag{39a}$$

$$\overline{n}_{x1}' = -\omega_0^2\overline{x}_1 - 2\omega_0\omega_1\overline{x}_0, \tag{39b}$$

$$\overline{y}_1'''' + 4\pi^2\overline{y}_1'' - \omega_0^2\overline{y}_1 = 2\omega_0\omega_1\overline{y}_0 + 2\pi\overline{n}_{x0}\cos 2\pi s, \tag{39c}$$

with

$$\overline{y}_1(0) = \overline{y}_1(1) = \overline{y}_1'(0) = \overline{y}_1'(1) = 0. \tag{39d}$$

We start by solving Eq. (39a). The boundary condition $\overline{x}_1(1) = 0$ implies

$$A_0 P_2(\omega_0) = 0, \tag{40}$$

with

$$P_2(\omega_0) \overset{\text{def}}{=} k_0^+ k_0^-((k_0^+ 2 - 2\pi^2)(\cos k_0^+ - \cosh k_0^-) + 2\pi^2(\cos k_0^+ \cosh k_0^- - 1)) + (k_0^+ 2k_0^- 2 + 8\pi^4)\sin k_0^+ \sinh k_0^-. \tag{41}$$

The solutions have to satisfy Eqs. (37) and (40), which are transcendental equations for ω_0. A numerical root finding analysis reveals that $P_1(\omega_0) = 0$ and $P_2(\omega_0) = 0$ share half of their roots, see Table 2 where columns with an even index correspond to common roots and match numerical values at $p = 4\pi^2$ for the continuous curves plotted in Fig. 3(d).

In the case of a common root, Eqs. (37) and (40) are fulfilled for non-vanishing A_0, and the corresponding modes have frequencies that are continuous in the control parameter close to buckling.

Table 2
First eight solutions of $P_2(\omega_0)=0$ (see Eq. (41)).

i	1	2	3	4	5	6	7	8
ω_0	0	44.36	169.4	182.1	390.6	398.8	688.5	694.6
k_0^+	2π	8.26	13.8	14.25	20.3	20.5	26.6	26.7
$(k_0^+ \bmod 2\pi)/(\pi/2)$		1.26	0.78	1.07	0.90	1.03	0.95	1.02
k_0^-	0	5.37	12.3	12.8	19.3	19.5	25.8	25.98

Table 3
First eight solutions of $P_3(\omega_0)=0$ (see Eq. (46)).

i	1	2	3	4	5	6	7	8
ω_0	0	44.36	74.4	182.1	259.4	398.8	517.4	694.6
k_0^+	2π	8.26	9.83	14.25	16.7	20.5	23.2	26.7
$(k_0^+ \bmod 2\pi)/(\pi/2)$		1.26	2.26	1.07	2.65	1.03	2.76	1.02
k_0^-	0	5.37	7.56	12.8	15.5	19.5	22.3	25.98

In the case of distinct roots, we are compelled to set $A_0=0$. In this case where $P_1(\omega_0)\neq 0$, we solve Eqs. (39a) and (39b) to obtain $\overline{x}_1(s)=0$ and $\overline{n}_{x1}(s)$ constant. The general solution of Eqs. (39c), (8.1) is then

$$\overline{y}_1(s)=\frac{2\pi\overline{n}_{x0}}{k_0^+\,2k_0^-2P_1(\omega_0)}[c_1k_0^+\cos k_0^+s-c_1k_0^+\cosh k_0^-s-c_2k_0^-\sin k_0^+s+c_2k_0^+\sinh k_0^-s+P_1(\omega_0)(\cos k_0^+s-\cos 2\pi s)], \tag{42}$$

where

$$c_1=k_0^-(\cos k_0^+-1)(\cosh k_0^-+1)+k_0^+\sin k_0^+\sinh k_0^-, \tag{43}$$

$$c_2=k_0^+\sin k_0^+(\cosh k_0^--1)+k_0^-(\cos k_0^+-1)\sinh k_0^-. \tag{44}$$

In order to select a mode, we need to proceed to order ε^2, which reads

$$\overline{x}_2'(s)=-\overline{y}_1'(s)\sin 2\pi s \quad \text{with } \overline{x}_2(0)=0=\overline{x}_2(1). \tag{45}$$

The boundary conditions at $s=1$ impose $P_3(\omega_0)/P_1(\omega_0)=0$ where

$$\begin{aligned}P_3(\omega_0)=&\,2k_0^-2k_0^+2(\cosh k_0^-\cos k_0^+-1)-4k_0^+(k_0^-2+k_0^+2)\sin k_0^+(\cosh k_0^--1)\\&+(4k_0^-(k_0^-2+k_0^+2)(1-\cos k_0^+)+4\pi^2k_0^-k_0^+\sin k_0^+)\sinh k_0^-.\end{aligned} \tag{46}$$

Oddly enough this function $P_3(\omega_0)$ has the same set of common roots as $P_1(\omega_0)$ and $P_2(\omega_0)$, see Table 3. The other roots correspond to the frequency values at which the (discontinuous) odd mode curves emerge from $p=4\pi^2$ in Fig. 3(d). Moreover one can verify that

$$P_3(\omega_0)=k_0^+k_0^-P_1(\omega_0)-8(k_0^+2+k_0^-2)\left(k_0^+\cos\frac{k_0^+}{2}\tanh\frac{k_0^-}{2}-k_0^-\sin\frac{k_0^+}{2}\right)\sinh k_0^-\sin\frac{k_0^+}{2}, \tag{47}$$

which implies that the common roots must verify:

$$\frac{k_0^+}{2}\tanh\frac{k_0^-}{2}=\frac{k_0^-}{2}\tan\frac{k_0^+}{2}. \tag{48}$$

These roots correspond to frequencies that do not vary abruptly after buckling has occurred. An approximate formula is $k_0^+\simeq\pi/2+2j\pi$ (with positive integers j), which yields $\omega_0\simeq(\pi/2)^2(4j+1)\sqrt{(4j-3)(4j+5)}$ (corresponding to columns with $i>1$ even in Table 3).

Formulas for the roots of the three functions P_1, P_2, and P_3 in the limit of large k_0^+ are given in Appendix C. In particular it is shown that the set of roots of P_3 which is not in common with P_1 and P_2 is such that $k_0^+\simeq 3\pi/2+2j\pi$ (with positive integers j). This implies that the frequencies emerging from buckling are such that $\omega_0\simeq(\pi/2)^2(4j+3)\sqrt{(4j+7)(4j-1)}$ (corresponding to columns with $i>1$ odd in Table 3).

9. Discussion

In [11] it is shown that, under certain hypotheses, in the zero thickness limit a slender cylinder behaves either as a flexible rod or as an extensible string and that one does not need to consider both bending and extension in a slender rod problem. Result in [11] was obtained for the statics of a clamped–free rod subjected to body and concentrated forces. We showed here that for displacement control clamped–clamped boundary conditions a model including both bending and extension is necessary to correctly describe the vibrations of the rod. One could then ask which constraint should be

relaxed in order to fall back into the results of [11]. We simply remark that in the load control case, see Appendix D, the inextensible limit is smooth and hence a model including bending alone correctly captures the vibrational behavior of the rod.

From a theoretical point of view, the singular inextensible limit in the displacement control case is rather surprising and unexpected. Indeed, Eqs. (13) can be easily recast in the form of a classical eigenvalue problem

$$\mathcal{L}\mathbf{X} = \omega^2 \mathbf{M}\mathbf{X}, \tag{49}$$

where $\mathbf{X}$ is the 6D vector build from the six normal mode variables, $\mathcal{L}$ is a first-order linear operator in $L^2([0,1])$ (the set of square integrable functions on the unit interval) and $\mathbf{M}$ is an inertia matrix. Therefore, a naive application of the classical theory of perturbation of eigenvalues for linear operators would suggest that once the eigenvalues have been found for a value of the parameter η, they can be locally continued in this parameter. That is we would expect the curves $\omega(p)$ of Fig. 3 to vary continuously as the parameter η is decreased to zero. While it is true for some curves, other curves behaves singularly in the $\eta \to 0$ limit. The fundamental mathematical reason for this phenomenon is that both the null spaces of the inertia matrix $\mathbf{M}$ and the linear operator $\mathcal{L}$ have a non-empty intersection in the inextensible ($\eta = 0$) case. Mathematically, the classical theory does not apply and new conditions for the analytic continuation of frequencies with respect to the parameters emerge. Some frequencies satisfy these relations (and hence can be analytically continued) while others do not. Finally, also due to the joint degeneracy of $\mathbf{M}$ and $\mathcal{L}$, there exists for $\eta = 0$ a continuous family of solutions at the critical load, given by an arbitrary increase along $\overline{n}_x$ (i.e. solutions of Eq. (27)). For larger values of the load but still at $\eta = 0$, some of these solutions are selected and emerge, apparently out of the blue. The mathematical structure of these linear problems and how they are related to various limits (nearly inextensible rods) deserves further attention.

A tentative classification for the modes is given by the number of nodes present in $0 < s < 1$, a mode i having $i-1$ nodes and i antinodes. We see that this classification works for the modes in the pre-buckling regime (Fig. 4), but fails for the third mode in the inextensible ($\eta = 0$) case (see shape B_3' in Fig. 10 and C_3' in Fig. 11), as well as in the extensible rod ($\eta > 0$) case provided we are far enough in the post-buckling regime (see shape C_3 in Fig. 6).

An interesting situation arises when the first mode intersects with the second mode. This can easily be obtained by computing an approximation of the buckled rod rise $Y_e(L/2)$ for which the first mode frequency $\omega^{(1)} \simeq 28 Y_e(L/2)/h$ meets the second mode frequency $\omega^{(2)} \simeq 44$. This happens for $Y_e(L/2) \simeq 1.6h$. At this height the shape of the fundamental mode changes from a single bump wave to a double bump wave. Anecdotically, we note that piano soundboards are precisely tuned in this parameter range (e.g. $h = 1$ cm, $L = 2$ m, and $Y_e(L/2) = 1$ cm). To which extent this toy model is relevant for the real problem of the piano soundboard and whether piano manufacturers are using the distinction between shallow shapes (where extension prevails) and deep buckled shapes (where bending prevails) to enrich the sound is a tantalizing idea that deserves further attention. We also note that in the case of the piano, the soundboard is a plate and not a rod, and that furthermore the soundboard is linked to the piano strings by a bridge, so really the whole system should be studied.

10. Conclusion

We have studied the in-plane vibrations of a slender extensible and shearable elastic rod around its post-buckled equilibrium configuration, in the displacement control case. We have shown that after buckling there is a narrow window in the loading parameter values in which half of the vibration frequencies vary abruptly. As the thickness of the rod is decreased, the vibration frequencies tend toward limiting values which do not correspond to what is found with a fully inextensible, unshearable model (i.e. an elastica). This mismatch present for half of the vibration frequencies has been found numerically and proved analytically. We conclude that we have identified a loading setup where the elastica model for slender rods fails to give the correct answer.

Acknowledgments

It is a pleasure to thank Olivier Thomas for discussions on Eq. (25). This publication is based in part upon work supported by Award no. KUK-C1-013-04, made by King Abdullah University of Science and Technology (KAUST) (A.G.). A.G. is a Wolfson/Royal Society Merit Award holder.

Appendix A. Closed form solution for the planar elastica

In the inextensible, unshearable case, the solution of system (10) with $\ddot{x}_e = 0$ and $\ddot{y}_e = 0$ corresponds to the equilibrium of the planar elastica, first studied by Euler [16] (see [17] for a historical account).

Closed-form solutions of these equations can be written in terms of elliptic functions, see e.g. [18]. In particular the dotted (red) curve in Fig. 2 has the parametric expression:

$$p = 16\, K(\lambda)^2, \tag{A.1}$$

$$d = 2\left(1-\frac{E(\lambda)}{K(\lambda)}\right)^2, \tag{A.2}$$

with $\lambda \in [0,1)$. The elliptic integrals are defined as $K(\lambda) = \int_0^{\pi/2}(1-\lambda\sin^2\theta)^{-1/2}\,\mathrm{d}\theta$ and $E(\lambda) = \int_0^{\pi/2}(1-\lambda\sin^2\theta)^{1/2}\,\mathrm{d}\theta$. Developing Eqs. (A.1) and (A.2) for $\lambda \ll 1$ yields Eqs. (31d) and (32) with $\varepsilon^2 = 4\lambda$.

Appendix B. Von Karman kinematics and 'strength of materials' notations

In Section 2, we have introduced the Cosserat–Kirchhoff notations where the normal force N_1 is related to the extension e_1 through the constitutive law (6) and where the current position (X,Y) of the central axis of the rod is given by (8a) and (8b), all these quantities being functions of the arc-length S of the reference configuration $(X_{\mathrm{ref}},Y_{\mathrm{ref}}) = (S,0)$. In 'strength of materials' notations one uses the displacements (see Fig. 1):

$$U = X-S, \quad V = Y \tag{B.1}$$

also functions of the arc-length S of the reference configuration. In the current configuration the derivative of the current position with regard to S will not yield a unit vector if extension occurs. If we restrict to the case where shear is not present (i.e. $e_2 = 0$), we have $X'(S)^2 + Y'(S)^2 = (1+e_1)^2$ which yields

$$U' + \tfrac{1}{2}V'^2 - e_1 = \tfrac{1}{2}(e_1^2 - U'^2). \tag{B.2}$$

Usually the right-hand side is neglected and the following von Karman approximation is used

$$U' + \tfrac{1}{2}V'^2 - e_1 \simeq 0. \tag{B.3}$$

Appendix C. Analytical formulas for the roots of the functions P_1, P_2, and P_3

In the limit of large k_0^+, that is in the limit of large $k_0^- = \sqrt{k_0^{+2}-4\pi^2}$ and high frequencies $\omega_0 = k_0^+ k_0^-$, we have

$$k_0^- \simeq k_0^+ - \frac{2\pi^2}{k_0^+} - \frac{2\pi^4}{k_0^{+3}} + O\left(\frac{1}{k_0^{+5}}\right). \tag{C.1}$$

Function $P_1(\omega_0)$ (see Eq. (38)) then reads:

$$P_1(\omega_0) \simeq \mathrm{e}^{k_0^-}[k_0^{+2}\cos k_0^+ + 2\pi^2(\sin k_0^+ - \cos k_0^+)] \tag{C.2}$$

and the solutions to $P_1(\omega_0) = 0$, for large k_0^+, are

$$k_0^+ \simeq \frac{\pi}{2} + \frac{1}{2j^2} + 2j\pi \quad \text{with } i = 2j, \tag{C.3}$$

$$k_0^+ \simeq \frac{3\pi}{2} + \frac{1}{2j^2} + 2j\pi \quad \text{with } i = 2j+1, \tag{C.4}$$

where j is a large integer, and i is the mode number (i.e. column number in Table 1). In the same limit of high frequencies, function $P_2(\omega_0)$ (see Eq. (41)) reads:

$$P_2(\omega_0) \simeq \tfrac{1}{2}\mathrm{e}^{k_0^-}[k_0^{+4}(\sin k_0^+ - 1) + 2\pi^2 k_0^{+2}\cos k_0^+ + 6\pi^4] \tag{C.5}$$

and the solutions to $P_2(\omega_0) = 0$, for large k_0^+, are

$$k_0^+ \simeq \frac{\pi}{2} - \frac{3}{2j^2} + 2j\pi \quad \text{with } i = 2j-1, \tag{C.6}$$

$$k_0^+ \simeq \frac{\pi}{2} + \frac{1}{2j^2} + 2j\pi \quad \text{with } i = 2j, \tag{C.7}$$

where j is a large integer, and i is the mode number (i.e. column number in Table 2). In the same limit of high frequencies, function $P_3(\omega_0)$ (see Eq. (46)) reads

$$P_3(\omega_0) \simeq \mathrm{e}^{k_0^-}[4k_0^{+3}(1-\sin k_0^+) + k_0^{+4}\cos k_0^+ + 2\pi^2 k_0^{+2}] \tag{C.8}$$

and the solutions to $P_3(\omega_0) = 0$, for large k_0^+, are

$$k_0^+ \simeq \frac{\pi}{2} + \frac{1}{2j^2} + 2j\pi \quad \text{with } i = 2j, \tag{C.9}$$

$$k_0^+ \simeq \frac{3\pi}{2} - \frac{4}{\pi j} + 2j\pi \quad \text{with } i = 2j+1, \tag{C.10}$$

where j is a large integer, and i is the mode number (i.e. column number in Table 3). We see that in this limit the three functions P_1, P_2, and P_3 share half of their roots, namely those given by (C.3)–(C.7) or (C.9).

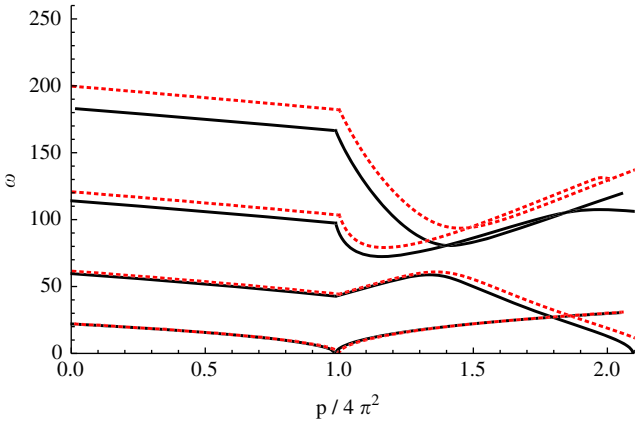

Fig. D.1. Frequencies for the lowest four vibration modes of a clamped–clamped rod around its fundamental and post-buckled equilibrium configurations, *in load-control boundary conditions*. Plain curves are for the extensible case with $\eta = 1/4800$, and dotted (red) curves are for the inextensible case ($\eta = 0$). (For interpretation of the references to color in this figure legend, the reader is referred to the web version of this article.)

Appendix D. Smooth inextensible limit in the load control case

We here show that in the case where the axial load p is controlled, the inextensible limit ($\eta \to 0$) is no longer singular. The boundary conditions for this case read:

$$x(0,t) = 0, \quad n_x(1,t) = -p, \tag{D.1a}$$

$$y(0,t) = 0, \quad y(1,t) = 0, \tag{D.1b}$$

$$\theta(0,t) = 0, \quad \theta(1,t) = 0. \tag{D.1c}$$

Vibrations of an inextensible rod are then possible before buckling as the right end is allowed to move axially. We see in Fig. D.1 that the inextensible case $\eta = 0$ is obtained as the smooth limit $\eta \to 0$ of extensible case, and that no mismatch is present (in particular there is a mode starting from $\omega = 0$ after buckling in the inextensible case).

References

[1] L.N. Virgin, *Vibration of Axially Loaded Structures*, Cambridge University Press, 2007.
[2] C. Touzé, O. Thomas, A. Chaigne, Hardening/softening behaviour in non-linear oscillations of structural systems using non-linear normal modes, *Journal of Sound and Vibration* 273 (2004) 77–101.
[3] N.C. Perkins, Planar vibration of an elastica arch: theory and experiment, *Journal of Vibration and Acoustics* 112 (1990) 374–379.
[4] S.T. Santillan, L.N. Virgin, R.H. Plaut, Post-buckling and vibration of heavy beam on horizontal or inclined rigid foundation, *Journal of Applied Mechanics* 73 (2006) 664–671.
[5] R.H. Plaut, L.N. Virgin, Vibration and snap-through of bent elastica strips subjected to end rotations, *Journal of Applied Mechanics* 76 (2009) 041011.
[6] P.H. Bilhuber, C.A. Johnson, The influence of the soundboard on piano tone quality, *Journal of the Acoustical Society of America* 11 (1940) 311–320.
[7] A. Mamou-Mani, J. Frelat, C. Besnainou, Numerical simulation of a piano soundboard under downbearing, *Journal of the Acoustical Society of America* 123 (2008) 2401–2406.
[8] A. Mamou-Mani, J. Frelat, C. Besnainou, Prestressed soundboards: analytical approach using simple systems including geometric nonlinearity, *Acta Acustica United with Acustica* 95 (2009) 915–928.
[9] A. Chaigne, C. Touzé, O. Thomas, Nonlinear vibrations and chaos in gongs and cymbals, *Acoustical Science and Technology* 26 (2005) 403–409.
[10] S.S. Antman, *Nonlinear Problems of Elasticity*, second ed., Springer-Verlag, New York, 2004.
[11] J.-J. Marigo, N. Meunier, Hierarchy of one-dimensional models in nonlinear elasticity, *Journal of Elasticity* 83 (2006) 1–28.
[12] S. Woinowsky-Krieger, The effect of an axial force on the vibration of hinged bars, *Journal of Applied Mechanics* 17 (1950) 35–36.
[13] N. Yamaki, A. Mori, Non-linear vibrations of a clamped beam with initial deflection and initial axial displacement, part I: theory, *Journal of Sound and Vibration* 71 (1980) 333–346.
[14] N. Yamaki, K. Otomo, A. Mori, Non-linear vibrations of a clamped beam with initial deflection and initial axial displacement, part II: experiment, *Journal of Sound and Vibration* 71 (1980) 347–360.
[15] A. Nayfeh, S. Emam, Exact solution and stability of postbuckling configurations of beams, *Nonlinear Dynamics* 54 (2008) 395–408.
[16] L. Euler, Methodus inveniendi lineas curvas maximi minimivi propreitate gaudentes, *Opera Omnia I* 24 (1744) 231–297.
[17] V.G.A. Goss, The history of the planar elastica: insights into mechanics and scientific method, *Science & Education* 18 (2009) 1057–1082.
[18] M. Nizette, A. Goriely, Toward a classification of Euler–Kirchhoff filaments, *Journal of Mathematical Physics* 40 (1999) 2830–2866.